Supplementary Information
On the mineral core of ferritin-like proteins: from archaea to mammals

A. García-Prieto[1,2], J. Alonso[2,3], D. Muñoz[4,5],
L. Marcano[5], A. Abad Díaz de Cerio[4,5], R. Fernández de Luis[2],
I. Orue[6], O. Mathon[7], A. Muela[2,4], M.L. Fdez-Gubieda[2,5]

[1] Dpto. de Física Aplicada I, Universidad del País Vasco - UPV/EHU, 48013 Bilbao, Spain
[2] BCMaterials, Parque tecnológico de Zamudio, 48160 Derio, Spain
[3] Department of Physics, University of South Florida, Tampa, FL 33647, USA
[4] Dpto. de Inmunología, Microbiología y Parasitología,
Universidad del País Vasco - UPV/EHU, 48940 Leioa, Spain
[5] Dpto. de Electricidad y Electrónica, Universidad del País Vasco - UPV/EHU, 48940 Leioa, Spain
[6] SGIker, Universidad del País Vasco UPV/EHU, 48940 Leioa, Spain
[7] European Synchrotron Radiation Facility, 38000 Grenoble, France

October 9, 2015

1 EXAFS analysis

We have measured the XANES spectrum of the FeIII-citrate. As it can be observed in figure 1, the XANES is completely different to that measured in prokaryotic samples.

We have also measured the XAFS spectra of the wild-type *E. coli* (control) grown in non-supplemented and iron supplemented media. Even though the repletion in both cases could be different, the XANES and EXAFS spectra are similar, see figure 2. As expected, we do not detect any change on the structure.

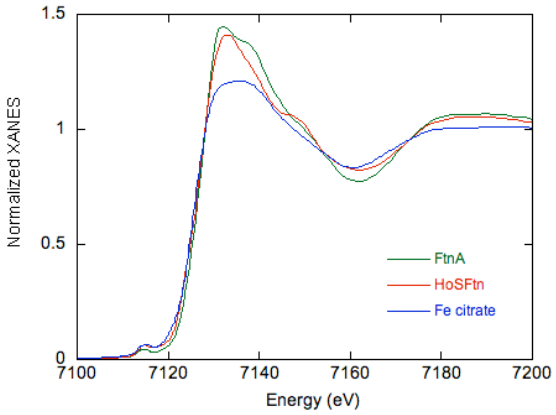

Figure 1: XANES spectra of Fe citrate compare with

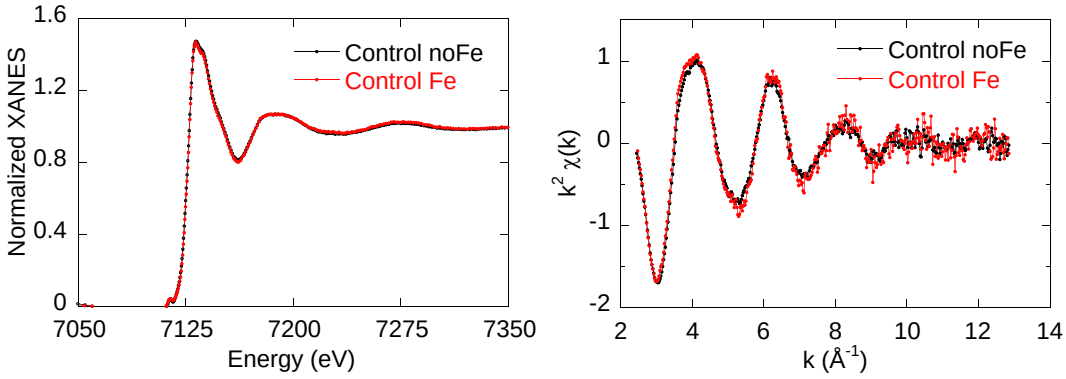

Figure 2: XANES spectra (left) and EXAFS spectra (right) of non-overexpressing *E. coli* DH5α (control) grown in non-supplemented and iron supplemented media

EXAFS spectra of the studied samples have been fitted to the expression: (*1*)

$$k\chi(k) = \sum_j S_0^2 N_j f_j(k,\pi) \frac{e^{-2\sigma_j^2 k^2} e^{-2\Gamma_j/k}}{R_j^2} \sin[2kR_j + \phi_j(k,\pi)]. \quad (1)$$

The sum expands over all the species of backscattering atoms at the same distance R_j of the central atom with variance σ_j^2 (Debye-Waller factor) around the absorber, and N_j is the number of such atoms. The scale factor S_0^2 is related to the many body effects and $e^{-2\Gamma_j/k}$ is a mean free path term that takes into account the inelastic losses of the photoelectron. $f_j(k,\pi)$ is the magnitude of the effective curved-wave backscattering amplitude for the jth type of atoms and $\phi_j(k,\pi) = (2\delta(k) - \pi) + \Phi_j(k)$, where the first and second terms represent the modification in the phase shift of the ejected photoelectron wave function by the potential of the central absorbing and backscattering atoms, respectively. In our case, the central atom is Fe and two types of scattering atoms have been taken into account: O and Fe and additionally P for the prokaryotic ferritins. The corresponding backscattering parameters $f(k,\pi)$, and $\phi(k,\pi)$ have been theoretically generated with the FEFF6.0 codes. (*2*) The fitting has been performed on the R space in 0 Å$\leq R \leq$ 3.5 Å. The fitting procedure consists on the minimization of the difference between the Fourier filtered experimental data $\chi_{exp}^F(k)$ and the model function $\chi_{th}(k)$. The function to minimize is defined as

$$S^2 = \frac{\sum_{i=1}^N [k_i^2 \chi_{exp}^F(k_i) - k_i^2 \chi_{th}(k_i)]^2}{\sum_{i=1}^N [k_i^2 \chi_{exp}^F(k_i)]^2} \quad (2)$$

In order to improve the reliability of the fits, the four samples have been fitted simultaneously as implemented in the IFeffit and Artemis softwares (*3,4*). The parameters S_0^2 and ΔE for each path were left free in the fitting procedure but were common for all the samples, resulting in a value of $S_0^2 = 0.8$. Results have been checked with the additional XAFS software Viper (*5*).

An attempt of fitting the EXAFS data to an amorphous function was made. In this case, the corresponding fitting expression in the framework of a the dense random packing model of hard spheres (*6*) is:

$$k\chi(k) = \sum_j S_0^2 N_j f_j(k) \frac{e^{-2\sigma_j^2 k^2} e^{-2\Gamma_j/k}}{R_j^2} \frac{1}{\sqrt{1+4k^2\sigma_{Dj}^2}} \sin\left[2kR_j + \arctan\left(2k\sigma_{DJ}\right) + \varphi_j(k)\right] \tag{3}$$

In this model, R_j is the distance between the centers of two touching spheres, and σ_{Dj} is the root mean square deviation of the distance between the absorbing atom and the neighbour j. This expression has proved to be very useful in the analysis of amorphous alloys, such as $(Fe_{0.2}Co_{0.8})_{75}Si_xB_{25\text{-}x}$, Co-P or Fe-B (*7–10*).

2 Transmission Electron Microscopy (TEM)

In figure**??** we show the TEM images taken at a PHILIPS CM120 microscope at the University of Basque Country, working at 120 kV for the wild-type *E.coli* (control), overexpressing bacterial ferritin (FTnA) and bacterioferritin (Bfr) grown in iron supplemented media. TEM analysis show isolated dense spots all over the cytoplasm in FtnA overexpressing cells and dense aggregates closed to the cytoplasmic membrane in Bfr overexpressing cells. However, this kind of dense spots and aggregates are not seen in the non-overexpressing E. coli DH5α. For HRTEM analysis we have focused on this particular events.

The lattice spacings and angular relationships obtained by the Fourier transform of HRTEM images of the HoSF have been compared with the theoretically generated patterns obtained from the defective free ferrihydrite model proposed by V.A. Drits and co-workers (*11*), Figure 4. Two possible zone axis, [1,1,1] and [0,1,1] have been correlated with the experimental data. Both of them possess four reflections with lattice spacing (2.43 Å, 2.39 Å) near the calculated value (2.47 Å), and two more with higher lattice spacing (2.50 Å) near the 2.56 Åvalue. The experimental angles (62° and 60°) also match with the theoretical ones (61.16° and 57.88°). The deviations between the experimental and theoretical data could be explained taking into

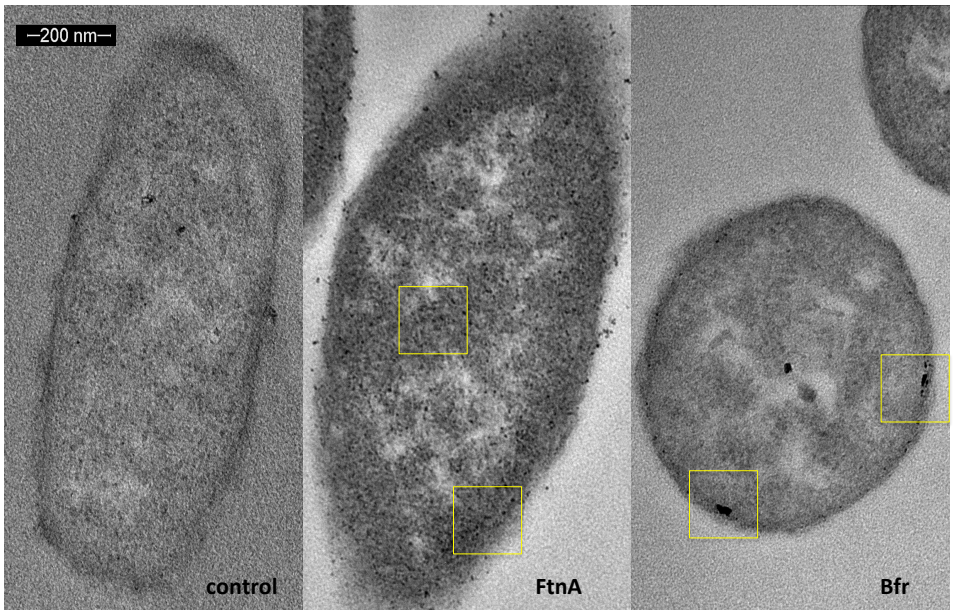

Figure 3: TEM images of the non-overexpressing *E.coli* (control), overexpressing bacterial ferritin (FTnA) and bacterioferritin (Bfr). The cells were grown in iron supplemented medium.

account that the ferritin cores are not exactly oriented in a zone axis. There is no possibility to identify exactly the zone axis in which the cores of the HoSF are oriented. Two HRTEM images in different zone axis, taken in the same HoSF core, are needed for this purpose. Nevertheless, the experimental and simulated patterns indicate that the nature of HoSF cores in related to the ferrihydrite.

The Figure 5a shows the Fourier transform of the bacterial ferritin core. The lattice spacings and angles between them are clearly different from those obtained for the HoSF. The Figure 5b indicates the mean spacing values and angle relationships between the spots observed in the Fourier transform image for the bacterial ferritin core.

3 Magnetic characterization

In a case of a paramagnet compound, Fe^{3+} should contribute with 5 μ_B which corresponds to a magnetic moment given by $J = 5/2$ and $g = 2$ (μ= gJ μ_B) In fact, this point has been confirmed by the fact that the magnetic data, M(H) and M(T), follow nicely a Brillouin function given by:

$$M = M_0 \frac{2J+1}{2J} \coth\left(\frac{2J+1}{2J}\frac{gJ\mu_B H}{k_B T}\right) - \frac{1}{2J}\coth\left(\frac{1}{2J}\frac{gJ\mu_B H}{k_B T}\right) + \chi H \qquad (4)$$

References

1. E. A. Stern *Contemp. Phys.*, vol. 19, no. 4, pp. 289–310, 1978.

2. S. I. Zabinsky, J. J. Rehr, A. Ankudinov, R. C. Albers, and M. J. Eller, "Multiple-scattering calculations of x-ray-absorption spectra," *Phys. Rev. B*, vol. 52, pp. 2995–3009, Jul 1995.

3. M. Newville, "*IFEFFIT*: interactive XAFS analysis and *FEFF* fitting," *J. Synchrotron Rad.*, vol. 8, pp. 322–324, Mar 2001.

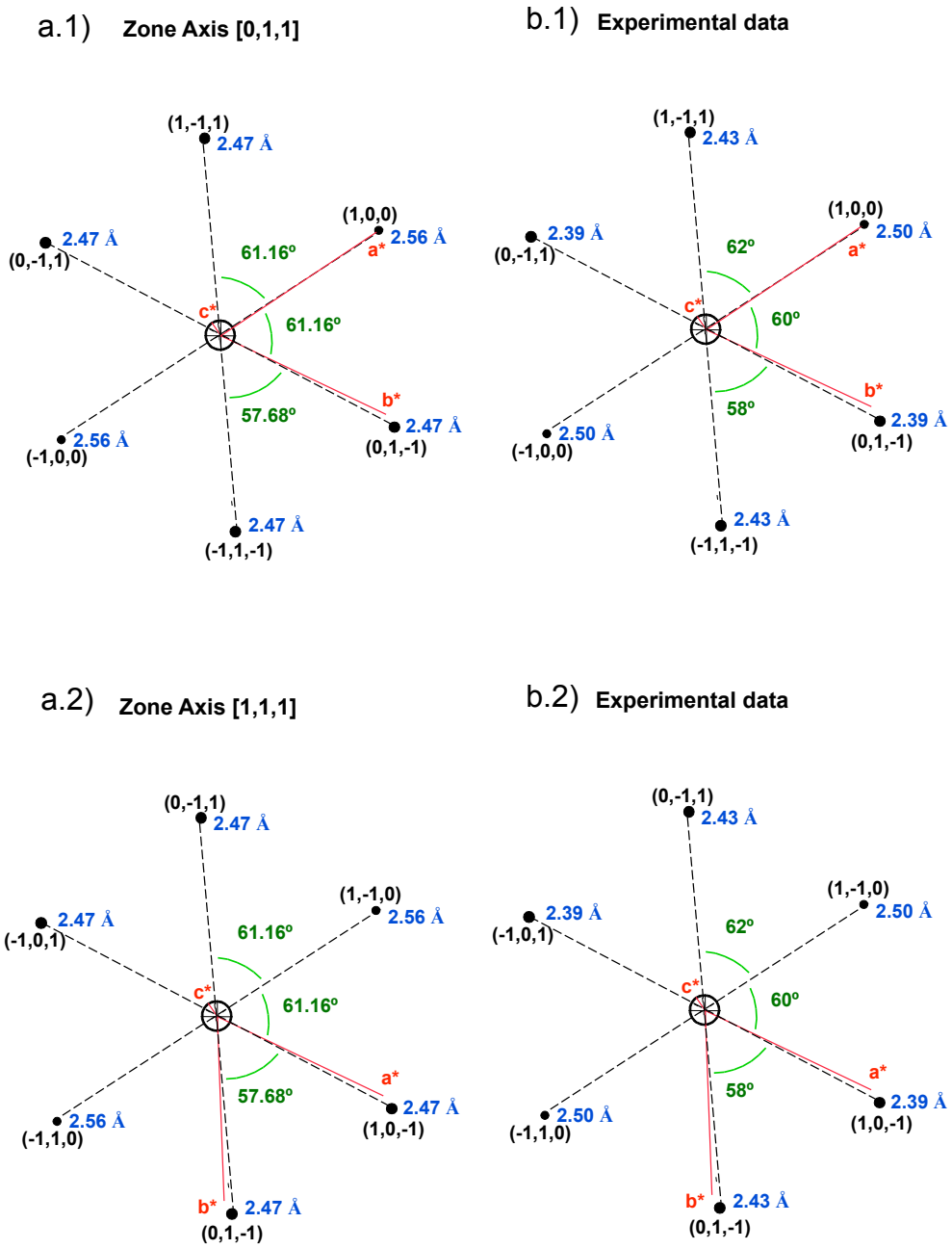

Figure 4: (a.1)-(a.2) Theoretical diffraction patterns for the defective free ferrihydrite, zone axis $[1, 1, 1]$ (a.1) and $[0, 1, 1]$ (a.2). (b.1)-(b.2) Spots of the Fourier transform of the HoSF indexed for a defective free ferrihydrite model in the $[1, 1, 1]$ (b.1) and $[0, 1, 1]$ zone axis.

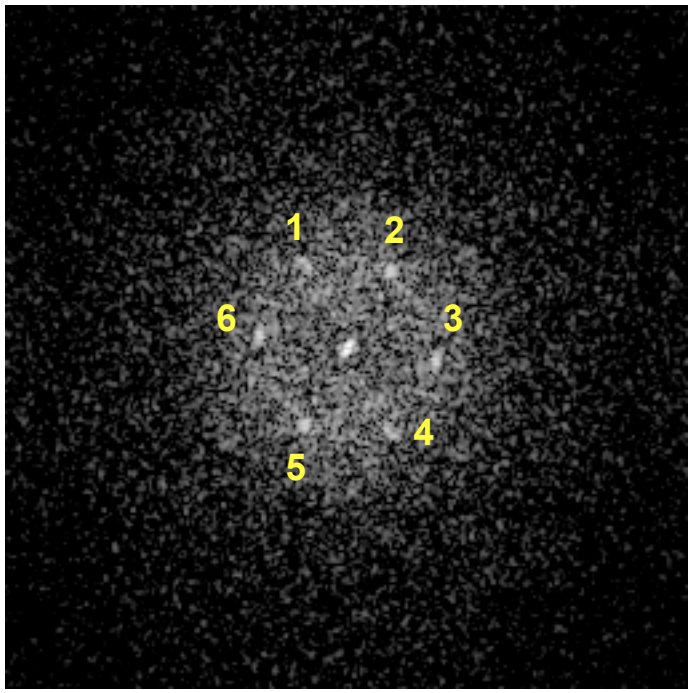

d_1(Å)	d_2 (Å)	angle°
2.88	2.87	68.0
d_2 (Å)	d_3(Å)	
2.87	2.57	55.8
d_3(Å)	d_4(Å)	
2.57	2.88	56.1
d_4(Å)	d_5 (Å)	
2.88	2.87	68.2
d_5(Å)	d_6(Å)	
2.88	2.57	55.8
d_6(Å)	d_1(Å)	
2.57	2.88	56.1

Figure 5: a) Fourier transform of the bacterial ferritin core. b) d spacing and angles for the observed spots.

4. B. Ravel and M. Newville, "*ATHENA*, *ARTEMIS*, *HEPHAESTUS*: data analysis for X-ray absorption spectroscopy using *IFEFFIT*," *J. Synchrotron Rad.*, vol. 12, pp. 537–541, Jul 2005.

5. K. V. Klementev, "Extraction of the fine structure from x-ray absorption spectra," *J. Phys. D Appl. Phys.*, vol. 34, no. 2, p. 209, 2001.

6. M. D. Crescenzi, A. Balzarotti, F. Comin, L. Incoccia, S. Mobilio, and N. Motta, "Exafs measurements on feb metallic glasses: Asymmetry of the radial distribution function," *Solid State Commun.*, vol. 37, no. 12, pp. 921 – 923, 1981.

7. M. L. Fdez-Gubieda, I. Orúe, F. Plazaola, and J. M. Barandiarán, "Evidence of strong short-range order in (fe0.2co0.8)75sixb25-x amorphous alloys from exafs spectroscopy," *Phys. Rev. B*, vol. 53, pp. 620–628, Jan 1996.

8. M. Fdez-Gubieda, A. García-Arribas, J. Barandiarán, R. López Antón, I. Orue, P. Gorria, S. Pizzini, and A. Fontaine, "Local structure and ferromagnetic character of fe-b and fe-p amorphous alloys," *Phys. Rev. B*, vol. 62, pp. 5746–5750, Sep 2000.

9. M. L. Fdez-Gubieda, A. García-Arribas, I. Orue, F. Plazaola, and J. M. Barandiarán, "Medium-range order as an intrinsic property of co-rich amorphous alloys," *Europhys. Lett.*, vol. 40, no. 1, p. 43, 1997.

10. A. García-Arribas, M. Fdez-Gubieda, and J. Barandiarán, "Comparative study of the structure and magnetic properties of co-p and fe-p amorphous alloys," *Phys. Rev. B*, vol. 61, pp. 6238–6245, Mar 2000.

11. V. A. Drits, B. A. Sakharov, A. L. Salyn, and A. Manceau, "Structural model for ferrihydrite," *Clay Miner.*, vol. 28, pp. 185–207, 1993.